Mouse mutant embryos overexpressing IGF-II exhibit phenotypic features of the Beckwith–Wiedemann and Simpson–Golabi–Behmel syndromes

Jonathan Eggenschwiler,[1] Thomas Ludwig,[2] Peter Fisher,[3] Philip A. Leighton,[4,5] Shirley M. Tilghman,[4] and Argiris Efstratiadis[1,6]

Departments of [1]Genetics and Development, [2]Anatomy and Cell Biology and [3]Pathology, Columbia University, New York, New York 10032 USA; [4]Howard Hughes Medical Institute and Department of Molecular Biology, Princeton University, Princeton, New Jersey 08544 USA

In mice, the imprinted *Igf2* gene (expressed from the paternal allele), which encodes a growth-promoting factor (IGF-II), is linked closely to the reciprocally imprinted *H19* locus on chromosome 7. Also imprinted (expressed from the maternal allele) is the *Igf2r* gene on chromsome 17 encoding the type 2 IGF receptor that is involved in degradation of excess IGF-II. Double mutant embryos carrying a deletion around the *H19* region and also a targeted *Igf2r* allele, both inherited maternally, have extremely high levels of IGF-II (7- and 11-fold higher than normal in tissues and serum, respectively) as a result of biallelic *Igf2* expression (imprint relaxation by deletion of *H19*-associated sequence) in combination with lack of the IGF2R-mediated IGF-II turnover. This excess of IGF-II causes somatic overgrowth, visceromegaly, placentomegaly, omphalocele, and cardiac and adrenal defects, which are also features of the Beckwith–Wiedemann syndrome (BWS), a genetically complex human disorder associated with chromosomal abnormalities in the 11p15.5 region where the *IGF2* gene resides. In addition, the double mutant mouse embryos exhibit skeletal defects and cleft palate, which are manifestations observed frequently in the Simpson–Golabi–Behmel syndrome, another overgrowth disorder overlapping phenotypically, but not genetically, with BWS.

[*Key Words:* IGF-II; *H19;* mouse mutant; overgrowth syndrome]

Received September 10, 1997; revised version accepted October 6, 1997.

Insulin-like growth factor II (IGF-II), a ligand that is important for normal embryonic growth, is encoded by the imprinted *Igf2* gene expressed only from the paternal allele in most tissues (DeChiara et al. 1991). The signaling of IGF-II is mediated by the type 1 IGF receptor (IGF1R; for review, see LeRoith et al. 1995; Rubin and Baserga 1995), whereas the type 2 IGF receptor (IGF2R) serves the degradation of excess IGF-II by receptor-mediated endocytosis (for review, see Ludwig et al. 1995). The *Igf2r* gene, residing on mouse chromosome 17, is imprinted and expressed exclusively from the maternal allele (Barlow et al. 1991).

In mice, *Igf2* is located on the distal region of chromosome 7 (see Beechey et al. 1997) at a distance of ~90 kb upstream from the reciprocally imprinted *H19* gene, which has the same transcriptional orientation and encodes a nontranslatable RNA of unknown function (Bartolomei et al. 1991; Zemel et al. 1992). The paternal *Igf2* and maternal *H19* alleles are expressed with similar tissue- and developmental-specificity using, at least in tissues of endodermal origin, the same enhancers located downstream from *H19* (Bartolomei et al. 1993; Leighton et al. 1995a). The linkage between *IGF2* and *H19* and their imprinted features are conserved in humans (chromosome 11p15.5; Zhang and Tycko 1992; Giannoukakis et al. 1993; Ohlsson et al. 1993).

Lack of IGF-II in heterozygous mice carrying a paternally transmitted *Igf2* targeted allele [*Igf2*(+/*p*−)] and in phenotypically indistinguishable *Igf2*(−/−) nullizygotes results in severe growth retardation (60% of normal birthweight; DeChiara et al. 1990, 1991). On the other hand, an abnormal increase in the amount of IGF-II in mouse mutants, either by a transcriptional or by a post-translational mechanism, results in overgrowth.

In mice carrying a maternally-derived 13-kb deletion mutation (*ΔH19*), which eliminates *H19* and 10 kb of upstream sequence (Leighton et al. 1995b), the normally silent maternal *Igf2* allele becomes transcriptionally active (imprint relaxation) and the increased amount of

[5]Present address: Department of Anatomy, University of California, San Francisco, California 94143 USA.
[6]Corresponding author.
E-MAIL arg@cuccfa.ccc.columbia.edu; FAX (212)923-2090.

mRNA from both alleles yields a higher-than-normal level of translation product resulting in increased birthweight (130% of normal; ''*H* phenotype''). Activation of the maternal *Igf2* allele, when the *ΔH19* mutation is in *cis*, is apparently caused by elimination of a negative imprinting signal, making possible an interaction between the intact 3′ enhancers and the normally dormant *Igf2* promoters (Leighton et al. 1995b).

Enhanced growth (140% of normal birthweight) is also a feature of *Igf2r*(−/−) nullizygotes or heterozygotes inheriting maternally a targeted disruption of the *Igf2r* gene [*Igf2r*(*m*−/+)] (Ludwig et al. 1996; see also Lau et al. 1994; Wang et al. 1994). In contrast to the *ΔH19* mutants, however, which are fully viable, the mice lacking IGF2R exhibit more severe abnormalities, including cardiac defects and edema, and usually die perinatally apparently of decompensated heart failure. These phenotypic manifestations (''*R* phenotype''), are due to overstimulation of IGF1R by excess of IGF-II resulting from the elimination of the IGF2R-mediated turnover mechanism, as demonstrated by genetic analyses using combinations of mutations (Ludwig et al. 1996; Louvi et al. 1997).

From the comparison of the *R* and *H* phenotypes, we surmised that absence of IGF-II degradation in mutants lacking IGF2R permits accumulation of ligand at a level higher than that attained by biallelic transcription in *ΔH19* mutants, also shown to exhibit incomplete imprint relaxation in some tissues, including the liver that contributes the circulating form of IGF-II (Leighton et al. 1995b).

It has often been postulated (see, e.g., Witte and Bove 1994), but not demonstrated formally, that excess of the growth-promoting activity of IGF-II during embryonic development is causally involved in the pathogenesis of the Beckwith–Wiedemann syndrome (BWS), a clinically variable disorder characterized by macrosomia, abdominal wall defects, macroglossia and other manifestations (for review, see Elliot and Maher 1994; Weng et al. 1995a). BWS is genetically heterogeneous and complex. The majority of BWS cases are sporadic and karyotypically normal, but ~15% are familial. In some families, linkage of BWS to the 11p15.5 region, where *IGF2* resides, has been demonstrated (Koufos et al. 1989; Ping et al. 1989; Ramesar et al. 1993). In addition, partial uniparental paternal isodisomies of 11p15.5 have been described in sporadic cases (Henry et al. 1991; Nyström et al. 1992), and also familial or sporadic 11p15 trisomies with paternal origin of the extra chromosomal material (Waziri et al. 1983; Turleau and de Grouchy 1985; Journel et al. 1985; Brown et al. 1991; Kubota et al. 1994).

From all of these observations, it was inferred that imprint relaxation or bipaternal *IGF2* expression could be involved in BWS pathophysiology, although biallelic transcription of *IGF2* was not always detected in examined cases (for review, see Weksberg and Squire 1996; Reik and Maher 1997). On the other hand, in 5/54 examined BWS patients, different loss-of-function mutations were described (some of them shown to be maternally inherited) in the imprinted $p57^{KIP2}$ gene encoding an inhibitor of cyclin-dependent kinases, which is located ~700 kb upstream from *IGF2* and is expressed preferentially from the maternal allele (Hatada et al. 1996; Lee et al. 1997; O'Keefe et al. 1997). $p57^{KIP2}$ mutations, however, cannot provide an explanation for BWS cases with 11p15 trisomy, in which the maternal $p57^{KIP2}$ allele should remain intact, and mouse mutants lacking $p57^{KIP2}$ (Yan et al. 1997; Zhang et al. 1997) did not exhibit any aspects of overgrowth, despite the appearance of some other hallmarks of BWS (see below). Conversely, despite their overgrowth resulting from excess of IGF-II, the *Igf2r* and *ΔH19* mutants did not simulate other aspects of the BWS phenotype.

To examine whether excess of IGF-II beyond the level reached with the *Igf2r* mutation could elicit additional BWS manifestations, we generated *Igf2r*/*ΔH19* double mutants and studied their phenotype (*R*/*H*), which was then compared with that of $p57^{KIP2}$ mutants, as both the $p57^{KIP2}$ and *IGF2* genes (and potentially other genes in the 11p15.5 region) could be involved in BWS pathogenesis. Our results, summarized for clarity in advance in Table 1, indicate that mutant embryos carrying a combination of the *Igf2r* and *ΔH19* mutations exhibit several BWS hallmarks and, in addition, some phenotypic characteristics of another genetic disorder, the Simpson–Golabi–Behmel syndrome (SGBS; see Weksberg et al. 1996). Although BWS and SGBS are distinct and variably manifested clinical entities of different etiology, they exhibit overlapping phenotypic features, including overgrowth and predisposition to tumors, to a degree that misdiagnosed cases are not uncommon (see Hughes-Benzie et al. 1992b; Verloes et al. 1995). SGBS is caused by mutations of the X-linked gene *GPC3,* encoding glypican-3 (a cell-surface heparan sulfate proteoglycan), which potentially binds and somehow sequesters or down-regulates IGF-II (Hughes-Benzie et al. 1996; Pilia et al. 1996).

Results and Discussion

Genetic crosses

Offspring inheriting maternally the *Igf2r* mutation [*Igf2r*(*m*−/+)] usually die perinatally (*R* phenotype), whereas the viability of overgrown *ΔH19* maternal heterozygotes [*ΔH19*(*m*−/+)] or nullizygotes [*ΔH19*(−/−)] (*H* phenotype) is normal. In contrast, paternal transmission of either the *Igf2r* or *ΔH19* mutation has no phenotypic consequences for the progeny. Accordingly, paternal heterozygous *Igf2r*(+/*p*−) males were first crossed with *ΔH19*(+/−) or *ΔH19*(−/−) females to derive among the progeny viable double heterozygotes [*Igf2r*(+/*p*−)/*ΔH19*(*m*−/+); *H* phenotype]. Of these offspring, female animals were mated with wild-type males to generate embryos belonging to four phenotypic classes (Table 2A)—normal (wild-type) embryos, mutants with *R* or *H* phenotype, and double mutants with *R*/*H* phenotype [*Igf2r*(*m*−/+)/*ΔH19*(*m*−/+)]. Additional breeding (Table 2B–D) increased the population of *R*/*H*, *H*, and *R* mutants at various developmental ages. In all of these

Table 1. *Comparison of phenotypic features*

	Patients[a]		Mutant mice[b]	
Manifestation	BWS	SGBS	*R/H* embryos	*p57^{KIP2}* mutants
Somatic overgrowth	128/215	42/47	+	−
Macroglossia	265/280	26/36	−	−
Abdominal wall defect				
omphalocele	170/282	1/40	+	(+)
umbilical hernia	56/174	15/40		+
Visceromegaly	23/44		+	−
hepatomegaly	35/41	13/30	+	−
nephromegaly	99/143	17/30	+	−
Renal dysplasia	13/22	−	−	+
Cardiac defect	29/148	18/42	+	−
Adrenal cytomegaly	17/18	−	−	+
Adrenal cysts	9/13	−	+	−
Skeletal abnormalities				
polydactyly	5/91	17/51	+	−
vertebral abnormalities	−	10/23	+	−
sternal abnormalities	−	[2]	+	+
Cleft palate	9/127	10/35	+	+
submucous cleft palate	2/10	9/35		
Lens abnormalities	−	−	+	+
Placentomegaly	11/12	[3]	+	−

[a]Data were compiled from original reports or reviews of nonoverlapping cases of BWS (Filipi and McKusick 1970; Sotelo-Avila and Singer 1970; Thorburn et al. 1970; Kosseff et al. 1976; Greenwood et al. 1977; Shapiro et al. 1982; McManamny and Barnett 1985; Niikawa et al. 1986; Pettenati et al. 1986; Takayama et al. 1986; Takato et al. 1989; Elliot et al. 1994; Weng et al. 1995b; Martínez y Martínez 1996) and SGBS (Simpson et al. 1975; Behmel et al. 1984, 1988; Golabi and Rosen 1984; Opitz 1984; Tsukahara et al. 1984; Neri et al. 1988; Opitz et al. 1988; König et al. 1991; Garganta and Bodurtha 1992; Gurrieri et al. 1992; Hughes-Benzie et al. 1992a, 1994, 1996; Chen et al. 1993; Yamashita et al. 1995). The frequency of occurrence of each manifestation (number of patients exhibiting a clinical feature as a fraction of total examined) is only indicative because of incomplete records. Expression of these numbers as percentages, which usually differ between literature reviews (see, e.g., Sotelo-Avila et al. 1980; Engström et al. 1988 for BWS), could be misleading. Rarely examined features are shown in brackets. Only phenotypic characteristics that can be compared with those of mutant mice are listed.

[b]The presence (+) or absence (−) of a phenotypic feature in mutant mice is shown. The data for *p57^{KIP2}* mutants are from Zhang et al. (1997).

crosses, we used 129/Sv wild-type males, whereas the genetic background of the females was mixed (129/Sv × C57BL/6J).

Embryonic lethality

The great majority of mutants lacking IGF2R die shortly after birth (Ludwig et al. 1996), but there is also a significant incidence of embryonic lethality from embryonic day 15.5 (E15.5) onward that is not observed among *ΔH19*(*m*−/+) mutants (Table 3). Interestingly, the combination of the *Igf2r* and *ΔH19* mutations (*R/H* phenotype) increased the frequency of lethality detected as early as E12.5 to a much higher level than was observed with single *Igf2r* mutant embryos. The mortality was increased with age, and no surviving double mutant embryos were recorded at E18.5 (Table 3).

Embryonic and also early postnatal lethality was also observed in *p57^{KIP2}* mutant mice. Two null mutations of the *p57^{KIP2}* gene have been described, and both analyzed in 129/Sv × C57BL/6 hybrids (Yan et al. 1997; Zhang et al. 1997). Despite some common phenotypic manifestations, however, dissimilarities were also observed, which could be attributed to significant differences in the genetic background of targeted AB2.1 (Zhang et al. 1997) and R1 (Yan et al. 1997) Embryonic stem (ES) cells derived from different 129/Sv substrains (see Simpson et al. 1997). A small fraction of embryos carrying either mutation died in utero, and all AB2.1/*p57^{KIP2}* mutants died at birth, whereas 11/87 (12.6%) of the R1/*p57^{KIP2}* mutants survived postnatally and did not exhibit abnormalities. Embryonic or early postnatal lethality has been described occasionally in BWS and SGBS (see, e.g., Hughes-Benzie et al. 1996; Ranzini et al. 1997).

Somatic overgrowth and placentomegaly

During gestation, the rate of growth (progressive increase in total cell number and, therefore, in size) of tissues, organs, and of the embryo as a whole, depends mainly on the rate of cell proliferation. In this regard, plots of total embryonic weight versus developmental age (growth curves) provide an average index of the overall growth process and are useful in the evaluation of relative growth rates.

Statistical and regression analyses of growth curve

Table 2. *Breeding data*

Phenotype	No. of embryos	Relative frequency observed	Relative frequency expected
A.			
Normal	114	1.17	1.0
H	92	0.95	1.0
R	85	0.87	1.0
R/H	98	1.01	1.0
B.			
H	27	0.95	1.0
R/H	30	1.05	1.0
C.			
Normal	138	1.0	1.0
H	139	1.0	1.0
D.			
Normal	44	1.13	1.0
R	34	0.87	1.0

(*A*) Crosses between *Igf2r*(+/−)/Δ*H19*(+/−) females and wild-type males. Data: 389 genotyped E12.5–17.5 embryos from 48 litters. (*B*) Crosses between *Igf2r*(+/−)/Δ*H19*(−/−) females and wild-type males. Data: 57 genotyped E13.5–18.5 embryos from 7 litters. (*C*) Crosses between Δ*H19*(+/−) females and wild-type males. Data: 277 genotyped E12.5–18.5 embryos from 32 litters. (*D*) Crosses between *Igf2r*(+/−) females and wild-type males. Data: 78 genotyped E12.5–18.5 embryos from 9 litters.

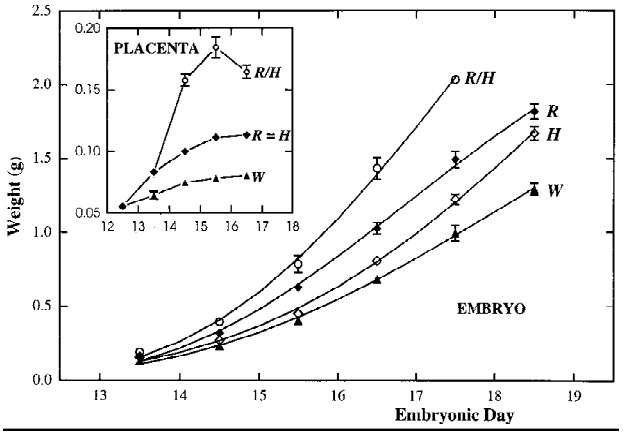

Figure 1. Embryonic growth kinetics. Plot of weights of wild-type (*W*) and mutant (*H*, *R*, and *R/H*) embryos vs. gestational age. The symbols correspond to average weights. For each time point, averages were calculated from a subset of the embryos listed in Table 2 (a total of 573 genotyped embryos of all classes and ages are represented). The width of the vertical bars represents 2 S.E.M.. The growth curves (lines connecting the symbols) are the results of regression analyses of average weights (see Materials and Methods). Growth curves of average placental weights (from a total of 541 weight measurements of placental specimens) are shown (*inset*). As expected, the placenta stops growing and actually loses weight toward the end of gestation (see McLaren 1965).

data for wild-type embryos and *H*, *R*, and *R/H* mutants (see Materials and Methods and Fig. 1) indicated that at E13.5 the normal embryos differed from all mutants, whereas the *H* and *R* embryos differed from *R/H* mutants, but not between them (normal < *H* = *R* < *R/H*). From E14.5 onward, however, all classes of embryos became distinct in size (normal < *H* < *R* < *R/H*). At E18.5, the weights of *H* and *R* embryos were 130% and 140% of normal, respectively, as described previously (Leighton et al. 1995b; Ludwig et al. 1996). At the most advanced ages that live *R/H* mutants could be recovered (E16.5 and E17.5), their sizes were dramatically larger than those of wild-type siblings (~200% of normal weight; see Fig. 1).

Table 3. *Frequency of embryonic death*

Embryonic age	Phenotype normal	*H*	*R*	*R/H*
E12.5	0 (0/45)	0 (0/35)	0 (0/19)	5.6 (1/18)
E13.5	0 (0/27)	0 (0/43)	0 (0/9)	5.3 (1/19)
E14.5	0 (0/54)	0 (0/46)	0 (0/24)	36.0 (9/25)
E15.5	0 (0/82)	1.9 (1/54)	4.2 (1/24)	58.8 (10/17)
E16.5	0 (0/57)	0 (0/47)	4.5 (1/22)	81.8 (27/33)
E17.5	0 (0/9)	0 (0/16)	12.5 (1/8)	87.5 (7/8)
E18.5	0 (0/22)	0 (0/17)	15.4 (2/13)	100.0 (8/8)

The percentages of total embryos found dead at each developmental age were calculated from the numbers shown in parentheses.

Body size differences (normal < *H* < *R* < *R/H*) were reflected in the absolute weights of various organs measured in E14.5–17.5 embryos, that is all mutants exhibited organomegaly, especially at more advanced ages (data not shown). Preliminary allometric regression analyses of organ and embryo weights (log–log plots) and pairwise analyses of covariance (data not shown; see Materials and Methods), however, indicated that the growth of the body and organs were not always proportional. Within the limitations of these results, we conclude that the weight increases of brain, lung, and gut followed quite closely the overall changes in mutant body weight. Other organs, however, exhibited particular deviations from normal allometry that were greater or less than expected relative to the increments in body size. Thus, the heart-to-body relationship observed in wild-type embryos was maintained in *H* mutants, but not in the *R* or *R/H* mutant classes (larger heart for the same embryonic weight; normal = *H* < *R* < *R/H*). In the case of the kidney, normal and *H* embryos again did not differ in allometry, whereas the *R* and *R/H* mutants exhibited a negative allometric relationship (normal = *H* > *R* = *R/H*; smaller kidney for the same embryonic weight, despite nephromegaly in absolute weights relative to normal beyond the age of E14.5). Finally, a third pattern of allometry was observed in the liver (normal < *H* < *R* = *R/H*).

Because it is known that excess IGF-II results in overgrowth of the placenta (Ludwig et al. 1996; Louvi et al. 1997), we also recorded placental weights (Fig. 1, inset). Statistical analysis of the data showed a difference in

average weights between wild-type and mutant placentas at E13.5 onward, but not at an earlier age (E12.5). Throughout gestation, however, differences in placental size were not detected between *H* and *R* mutants, whereas the placentas of *R/H* mutants were much heavier starting at E14.5. Thus, at the peak of placental growth (E15.5), the size of *H* and *R* placentas was ~140% of normal, whereas in *R/H* mutants the corresponding size exceeded 230% (E16.5 placentas are shown in Fig. 1, inset).

Somatic overgrowth and organomegaly, and also placentomegaly whenever recorded, are frequent features of both BWS and SGBS (Table 1), whereas the $p57^{KIP2}$ mutants lack such manifestations. In contrast to the *R/H* embryos, however, which have histologically normal kidneys (data not shown), the $p57^{KIP2}$ mutants exhibit renal medullary dysplasia analogous to that observed in BWS patients.

Omphalocele

From E12.5–E13.0 of mouse development, there is a physiological umbilical hernia; loops of the midgut protrude through the abdominal wall at the umbilicus. At E15.5, the intestine begins to return to the peritoneal cavity, and the body wall closes by E16.5 (only the umbilical cord and its contents remain in this region; Pleeging 1977; Kaufman 1992). A similar physiological umbilical hernia is transiently present in the human embryo (see Duhamel 1963; Achiron et al. 1995; Vermeij-Keers et al. 1996). By the 10th to 12th gestational week, however, the gut returns to the abdominal cavity and the apices of cephalic, caudal and lateral folds forming the coelom come together at the umbilical ring. Failure of the intestine to return to the coelom results in an umbilical hernia (Achiron et al. 1995). In this ventral wall defect, the folds develop normally, the umbilical ring is intact, the protrusion is covered with skin, and the herniation does not include any organ other than midgut present inside the umbilical cord. An omphalocele (exomphalos), on the other hand, results from a failure of the lateral folds to progress (Duhamel 1963; Achiron et al. 1995). Thus, the ventral wall defect is large and an umbilical ring is not formed. The large protrusion includes not only intestine, but also liver and sometimes other viscera enveloped by a transparent sac consisting of an internal lining of peritoneum and an external thin covering of amnion (skin is not present).

When embryos were examined at E16.5, a time at which the physiological umbilical hernia has been resolved completely in normal mice, a striking feature of *R/H* mutants was the presence of a large omphalocele in 20/22 specimens (Fig. 2B,C), consisting of a large portion of the liver always present anteriorly and intestinal loops lying posteriorly (Fig. 2E,G; cf. with D and F). In transverse sections, the histologically normal abdominal muscle and skin layers were seen as extending only to the borders of the sac covering the herniation (Fig. 2E). A smaller omphalocele was observed in 7/22 *R* embryos and consisted either of protrusion of only a small portion of the liver (five specimens) or of a mild herniation of only the gut (two specimens). An omphalocele was never observed in wild-type or *H* embryos (57 and 47 specimens, respectively).

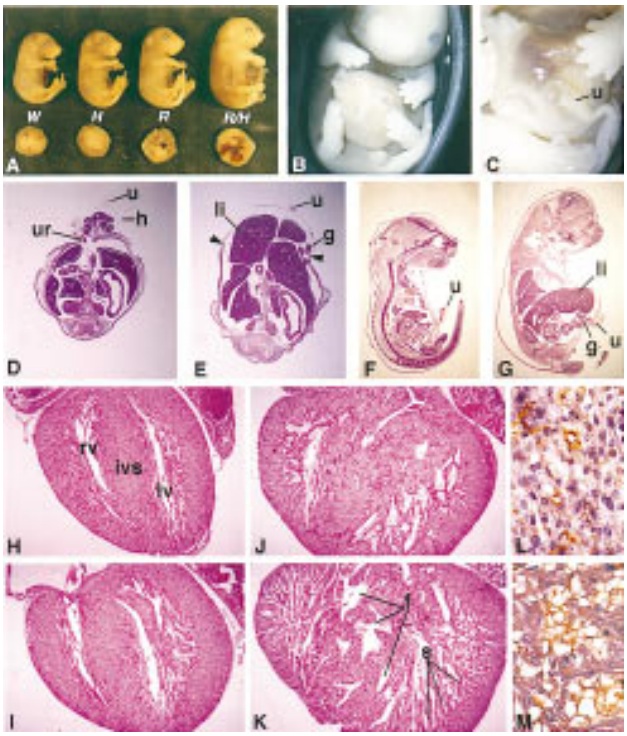

Figure 2. Anatomical data and cardiac histopathology. (*A*) The external appearances of wild-type and mutant littermates and their placentas are compared at E16.5, to demonstrate the overgrowth of mutant embryos. (*B*) Ventral view of an E16.5 *R/H* mutant embryo with a large-size omphalocele. A blow-up of the transparent omphalocele sac of another double mutant (E16.5) is shown in *C*. The herniated liver is visible through the sac wall. The umbilical cord (u) is located on the apex of the sac. (*D*) Transverse section through the abdomen of a wild-type E15.5 embryo showing the physiological hernia (h) of the midgut at this age. One side of the umbilical ring (ur) is noted. A corresponding section of an *R/H* mutant embryo with an omphalocele is shown in *E*, to demonstrate the failure of lateral folds forming the coelom to close ventrally over the viscera. Arrowheads indicate the points where the muscle and skin layers of the abdominal wall terminate leaving the herniated liver (li) and gut (g) covered only with a thin sac of peritoneum and amnion. (*F,G*) Sagittal sections of E16.5 wild-type and *R/H* mutant embryos, respectively. The large portion of herniated liver and the pronounced edema on the dorsal side of the double mutant are notable. (*H–K*) Coronal heart sections of wild-type, *H*, *R*, and *R/H* embryos at E17.5, respectively. The right and left ventricles (rv and lv) and the interventricular septum (ivs) are shown. Sinusoids (s) of increasing prominence ($W < H < R < R/H$) are present in the ventricular walls and have become invasive in the septum of *R/H* mutants (*K*) resulting in fenestration (f). (*L,M*) Anti-PECAM staining (brown) of endothelial cells in the myocardium of wild-type and *R/H* embryos, respectively. These cells are very abundant in the mutants and have formed a network within the trabeculae of the muscular cardiac wall counterstained with hematoxylin.

Abdominal wall defects were also observed in $p57^{KIP2}$ mutants. The intestine was short and abnormal in 40/87 (46%) of the mice carrying the R1/$p57^{KIP2}$ mutation, but umbilical hernia was observed in only 1/87 specimens (Yan et al. 1997). The incidence of umbilical hernia appeared to be higher in AB2.1/$p57^{KIP2}$ mutants, and malformed intestines located in part in front of the liver were found on occasion outside of the abdominal cavity. Herniation was associated with dysplasia of the muscles of the body wall, which did not reach the midline of the abdomen in the mutants. The occurrence of omphalocele or umbilical hernia is very high in BWS, whereas in SGBS only the latter defect appears frequently (Table 1).

Cardiac abnormalities

Previously, comparative histopathological analysis of *R* embryos and normal siblings at E18.5 (Ludwig et al. 1996) had shown a dramatic enlargement of the heart in the mutants, characterized by ventricular mural thickening and cavity dilatation, apparently attributable to hyperplasia of cardiomyocytes (increase in cell number), as the size of these cells was normal (absence of hypertrophy). An additional prominent feature of abnormal development was the persistence of early embryonic sinusoids observed in the ventricles and extending to the septa. During heart morphogenesis (for review, see Brutsaert and Andries 1992; Icardo and Manasek 1992), endothelial endocardial cells invaginate into the inner zone of the myocardium from E10.0 onward, forming interlinked streaks of heart muscle invested with endothelium (trabeculae) and a network of intertrabecular spaces (sinusoids). Before the development of coronary capillaries in the epicardium that become functional at E13.5, the sinusoids serve as primitive vessels, but regress and disappear later in development, when the trabeculae are incorporated into the ventricular wall.

Coronal, transverse and sagittal heart sections in normal embryos and mutants with *H*, *R*, and *R/H* phenotypes were examined at E16.5 (four specimens for each class) and E17.5 (one specimen for each class). Although a few sinusoids were observed in the ventricles of wild-type embryos, the number of these channels was much more pronounced in *R* and especially in *R/H* embryos, whereas the *H* mutants did not exhibit a striking difference from the controls (Fig. 2H–K). In *R* and, more prominently, *R/H* mutants, sinusoids were observed not only in the ventricular walls but also in the septa. Hyperplasia of the muscular wall was a common feature of the mutants (*H* < *R* < *R/H;* see Fig. 2H–K).

The intertrabecular spaces in the ventricles of the double mutants were filled with a network of hyperplastic endothelial cells, as confirmed by positive staining with an anti-PECAM antibody (Fig. 2M). Such cells were also observed within the atria (data not shown). In *R* embryos, these features were less pronounced, especially in the atria. Even less pronounced were the endothelial-type cells in *H* embryos, observed in the ventricles of two of four specimens. The number of endothelial cells in the ventricles of wild-type embryos was comparatively much smaller (Fig. 2L). Communication between the ventricles (ventricular septal defect; VSD) was observed in three of four *R/H* specimens, and appeared to be a fenestration-type defect of the septum due to invasive sinusoids (Fig. 2K). We note that the aortic and pulmonary valves were large and thickened in *R/H* mutants, while two of four of these specimens exhibited signs of accumulation of pericardial fluid. *R/H* embryos had an edematous external appearance similar to that described for *R* mutants (Ludwig et al. 1996). Previously, we speculated that precise modulation of IGF-II levels may be a requirement for unperturbed cardiogenesis (see Ludwig et al. 1996). In this regard, the presumably uncontrolled excess of IGF-II in *R* and *R/H* mutants, which results in dramatic hyperproliferation of cardiomyocytes, could potentially bring growth and morphogenesis out of pace.

Whereas $p57^{KIP2}$ mutants are free of cardiac defects, such abnormalities are not rare in BWS and SGBS patients (Table 1). Although specific details are available only occasionally, VSDs have been reported in several cases of both syndromes (see, e.g., Greenwood et al. 1977; Hughes-Benzie et al. 1996). Their pathogenetic correspondence, however, if any, to the VSDs observed in *R/H* mutants is unknown. On the other hand, the persistence of sinusoids in all mutants that we examined, also reported in some cases of human heart abnormalities (see, e.g., Amann and Sherman 1992), was never described in BWS or SGBS to our knowledge.

Skeletal abnormalities

All three classes of mutants examined in this study exhibited polydactyly (i.e., presence of supernumerary digits), whereas the *R* and *R/H* embryos also exhibited abnormalities of the sternum. Additional skeletal defects involving the vertebrae, however, were exclusively a feature of the double mutants. Sternal anomalies (Wang et al. 1994) and polydactyly analyzed in less detail were reported previously for mutants lacking IGF2R (Wang et al. 1994; Lau et al. 1994; Ludwig et al. 1996). Polydactyly was not observed previously in *H* mice (129/Sv × C57BL/6 hybrids; Leighton et al. 1995b), but was now detected apparently because of an increase of the 129/Sv component in the genetic background (see Genetic crosses, above). Thus, after breeding into the 129/Sv background for three generations, 12/12 *H* mutants exhibited postaxial polydactyly (data not shown).

In some human polydactylies taken into consideration for comparison, the extra digit may be present on the postaxial (ulnar or fibular) or preaxial (radial) side of the extremities (Temtamy and McKusick 1978). In Type A postaxial polydactyly, the extra digit is rather well developed, although it may consist of only two phalanges, whereas in Type B it is rudimentary and does not always include a phalangeal skeletal element. In preaxial polydactyly of the thumb, there is bifurcation of the distal phalanx or duplication of a skeletal component.

The postaxial polydactyly manifested in all classes of mutants was not observed in wild-type embryos, as ex-

pected (see Table 4; Fig. 3A). The penetrance of this trait was incomplete in *H* embryos, but complete or almost complete in *R/H* and *R* mutants, whereas the expressivity in terms of severity and number of affected limbs was variable and increased in the order *H* < *R* < *R/H* embryos (Table 4). Overall, extra digits appeared with preference for forelimbs over hindlimbs and for the right over the left side (Table 4). Examination of forelimbs in skeleton preparations stained with alizarin red and alcian blue showed that the postaxial polydactyly of *H* mutants was Type B-like; the extra digit was small and contained a single phalangeal bone (Fig. 3B). The same malformation appeared in some *R* and *R/H* mutants, whereas others (the minority of *R* embryos and the majority of *R/H* embryos) also exhibited Type A-like extra digits with two phalanges (see Table 4 and Fig. 3C). In an examined *R/H* case, a third skeletal element was present, which, because of its position, could be a rudimentary metacarpal (Fig. 3D). Preaxial polydactyly consisting of a doubling or bifurcation of the distal phalanx of the pollex (thumb) was observed in association with postaxial polydactyly in a small minority of *R* mutants and in most double mutants (Fig. 3E) but never in *H* embryos. Morphologically, the doubling ranged from two completely separate cartilaginous condensations to a single broad phalanx with two connected condensations.

In rodents, *Igf2* is expressed in proximal limb bud mesoderm and at a lower level in rapidly proliferating undifferentiated mesodermal cells beneath the surface ectoderm at ~E12.0. Subsequently, this transcription becomes restricted to primordial skeletal condensations

Table 4. *Postaxial polydactyly*

	Normal	*H*	*R*	*R/H*
Embryos examined	45	41	47	26
Polydactylous	0	28[a]	44[b]	26[c]
embryos (%)	(0)	(68.3)	(93.6)	(100)
Extra digits in				
right forelimb		9	6	0
both forelimbs		18	15	3
right forelimb and right hindlimb		0	0	1
both forelimbs and right hindlimb		1	6	2
both forelimbs and left hindlimb		0	1	0
all four limbs		0	16	20

[a]In 22 of the polydactylous *H* embryos examined in more detail, the postaxial polydactyly consisted of a single phalanx. Associated preaxial polydactyly was not observed.

[b]In a subset of polydactylous *R* embryos that were examined, the postaxial polydactyly consisted either of a single phalanx (20/29) or of two phalanges (9/29; in the right forelimb in 8 specimens and in both forelimbs in 1 specimen). Associated preaxial polydactyly was observed in 2/29 embryos (in the right forelimb in 1 specimen and in both forelimbs in the second specimen).

[c]In a subset of polydactylous *R/H* embryos that were examined, the postaxial polydactyly consisted either of a single phalanx (1/10) or of two phalanges (9/10; in the right forelimb in 3 specimens and in both forelimbs in 6 specimens). Associated preaxial polydactyly was observed in all 9 of the latter embryos (in the right forelimb in 3 specimens and in both forelimbs in 6 specimens; combination of the features of preaxial polydactyly and postaxial polydactyly with two phalanges in both forelimbs was observed in 5 cases).

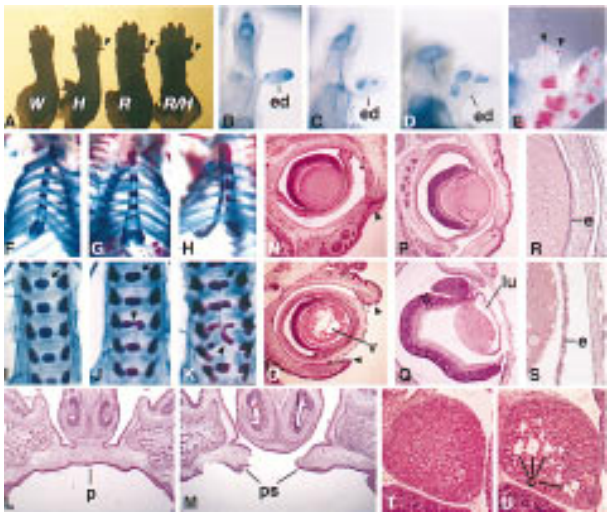

Figure 3. Skeletal, palatal, lens, and adrenal abnormalities. (*A*) Right forelimbs of E16.5 wild-type and mutant embryos shown in silhouette, to demonstrate the increasing degree of manifestation of postaxial polydactyly in the mutants (*H* < *R* < *R/H*). (*B–K*) Regions of skeletons stained with alizarin red and alcian blue (E16.5, *B–D;* E17.5, *E–K*). The postaxial extra digit (ed) in the right forelimb consists of a single cartilaginous skeletal element in an *H* mutant (*B*), two elements (phalanges) in an *R* mutant (*C*), and three elements (two phalanges and a possible extra metacarpal) in an *R/H* mutant (*D*). (*E*) Preaxial polydactyly of an *R/H* mutant (the arrowheads indicate the bifurcated distal phalanx of the pollex). (*F–H*) Sternal regions of skeletons from wild-type, *R*, and *R/H* embryos, respectively. The sternum is broad and has a bifurcating xiphoid process in the *R* mutant (*G*), whereas it is split in the *R/H* mutant (*H;* for details, see text). (*I–K*) Regions of lumbar vertebrae of the same skeletons as in (*F–H*). An arrow marks the first lumbar vertebra (L_1). An arrowhead in *J* indicates fusing twin ossification centers in L_3 of an *R* mutant. An arrowhead in *K* indicates unilateral longitudinal fusion between half ossification centers in L_3 and L_4. (*L,M*) Coronal sections of heads of E16.5 wild-type and *R/H* embryos, respectively. Fusion of the palate (p) has occurred in the normal embryo (*L*), whereas the palatal shelves (ps) are unfused (cleft palate) in the double mutant (the tongues have been removed before sectioning). (*N,O*) Coronal and (*P,Q*) sagittal sections of eyeballs of wild-type (*N,P*) and *R/H* (*O,Q*) embryos. Arrowheads in *N* and *O* indicate fused and open eyelids, respectively. In the double mutant, the lens has a ''vacuolated'' (v) appearance (*O*) in coronal sections because the lumen (lu) remains unfilled (lack of contact between lens fibers and epithelium; *Q*). (*R,S*) Same as *P* and *Q*, but at a higher magnification to demonstrate the disorganization of lens epithelium (e) in the *R/H* mutant (*S*). (*T,U*) Sections of adrenal glands of wild-type and *R/H* embryos, respectively, to demonstrate the occurrence of cysts (c) in the double mutants.

(digital rays; Streck et al. 1992). Interestingly, alterations in growth rate and excess of mesenchymal cells that could condense spontaneously have been proposed as a possible mechanism involved in the appearance of extra digits (Dollé et al. 1993). Thus, the polydactyly induced by IGF-II overexpression may be eventually correlated to hyperproliferation resulting in imbalance of the reciprocal, complex interactions between the ectoderm and the underlying mesenchyme involved in outgrowth and patterning of the developing limb bud (for review, see Laufer 1993; Cohn and Tickle 1996).

Sternal defects were observed in *R* and *R/H* mutants (Fig. 3G,H), but not in normal embryos (Fig. 3F) or *H* mutants (data not shown). The sternum consists of the manubrium, four sternebrae and the xiphoid process (xiphisternum) that is cartilaginous in its lower half. The sternum develops from E12.5 onward from a pair of mesodermal condensations that elongate caudally, move toward each other, fuse in the midline and then differentiate into cartilage by E16.0 (Chen 1952). Ossification centers, one each for the lower part of the manubrium and the upper three sternebrae, and two pairs for the fourth sternebra and the xiphisternum, appear at E17.0–E17.5 (Kaufman 1992). In a stained skeleton preparation of an *R* mutant examined at E17.5, the ossification centers of the fourth sternebra had not fused in the midline and were underdeveloped in comparison to the wildtype, whereas the similarly unfused centers of the xiphisternum were very broad (Fig. 3G). Otherwise, the upper portion of the sternum appeared normal. In contrast, the sternum of *R/H* mutants of the same age was split along the entire midline and almost duplicated in total width (Fig. 3H), suggesting that fusion of the sternal rudiments had not occurred. Similar observations were made in skeletons of E16.5 *R* and *R/H* embryos (two each).

Vertebral abnormalities were observed in the lumbar region of an *R/H* embryo examined at E17.5 (Fig. 3K). Ossification of all vertebrae occurs from three centers, one in each half of the arch and one in the vertebral body, all present in the lumbar region by E16.0 (Kaufman 1992). Although the ossification centers of the arch appeared normal in *R/H* mutants, ossification in the body of the last thoracic vertebra (T_{13}) and lumbar vertebrae L_1–L_4 appeared to be initiated from asymmetrical bilateral centers rather than from a single one in the middle (Fig. 3, cf. I and K). The twin centers in L_2 were fused in the midline, whereas they were still separate in L_3–L_4. Interestingly, in the latter two vertebrae, unilateral longitudinal fusion had occurred between the adjacent half centers (Fig. 3H). Had the *R/H* embryos survived and developed further, this abnormal morphogenetic process would have resulted in a double (fused) hemivertebra on one side and two single hemivertebrae on the other side. In the lumbar region of an *R* mutant, only a single occurrence of fusing twin centers was observed in L_3 (Fig. 3J). Similar vertebral anomalies were observed in skeletons of E16.5 *R* and *R/H* embryos (two each).

The *p57^{KIP2}* null mutants exhibited endochondral bone ossification defects and an unfused sternum very similar morphologically to that observed in *R/H* embryos (Zhang et al. 1997). On the other hand, polydactyly or vertebral abnormalities other than ossification delays were not observed in the absence of p57^{KIP2}.

Although postaxial polydactyly is a rare feature of BWS (Table 1), other significant skeletal abnormalities were not reported (see Lee 1972) and only advanced bone age was noted quite frequently. In contrast to BWS, polydactyly is relatively frequent in SGBS patients (Table 1), but few details have been described and only occasionally. Interestingly, the occurrence of vertebral fusions, hemivertebrae and bifid xiphisternum in SGBS has also been reported (Table 1).

Cleft palate

Development of the mouse secondary palate begins at E12.0 with the formation of bilateral palatal shelves arising from the maxillary processes, which grow vertically along the sides of the tongue (E13.0), elevate to a horizontal plane over the tongue (E14.0–14.5) and finally extend towards the midline and fuse completely by E15.5 (Ferguson 1988; Kaufman 1992). Morphogenetic perturbation at any one of these steps results in palatal clefting.

Examination of E15.5–E17.5 embryos showed that complete palatal fusion had occurred in wild-type specimens (11; Fig. 3L) and also in *H* mutants (10) and in *R* mutants (11) without exception. In contrast, 5/10 *R/H* mutants had cleft palate (two of four at E15.5, two of five at E16.5 and one at E17.5; Fig. 3M). The occurrence of cleft palate in some of the mice carrying an *Igf2* transgene in the homozygous state has been described (Wise and Pravtcheva 1997). *Igf2* mRNA is expressed transiently and uniformly in palatal mesenchyme, after elevation of the palatal shelves and before their fusion (E14.0), whereas the IGF-II peptide is localized in palatal epithelia suggesting a paracrine role (Ferguson et al. 1992). The involvement of IGF-II in the pathogenesis of cleft palate in *R/H* mutants, however, is unclear. Interference of the tongue in palatogenesis is excluded, because elevation of the palatal shelves is apparently normal and macroglossia is not a feature of these mutants. Perhaps, a simple explanation is that disproportionate and/or faster overgrowth increasing the width of the oronasal cavity does not permit contact and fusion of the palatal shelves in *R/H* embryos.

Cleft palate was also observed in *p57^{KIP2}* mutants (41/87: 47%; Yan et al. 1997; see also Zhang et al. 1997). Cleft palate is a rare feature of the BWS phenotype, but appears quite often in SGBS patients (Table 1).

Eye abnormalities

In mouse embryos, the eyelids begin forming at E13.0, fuse with each other progressively through a process that is completed by E17.0, and reopen approximately on the 14th postnatal day, when the connecting epithelium breaks down (see Harris and McLeod 1982). In wild-type and *H* embryos examined at E16.5 (11 specimens each), the eyelids were fused, whereas they were open in 5/14 *R* embryos and 12/13 *R/H* embryos. At E17.5, however,

R embryos (eight of eight examined) exhibited fused eyelids, whereas the eyelids of a single *R/H* mutant recovered at this age were open (Fig. 3O). Because double mutants do not survive beyond E17.5, it is not possible to ascertain whether the process of eyelid fusion is impaired or simply developmentally delayed, but to a greater extent than that observed in *R* embryos. The latter possibility appears to be more likely, as a single E16.5 *R/H* embryo with fused eyelids was recovered.

R and *R/H* mutants also manifested an abnormal lens phenotype. In E11.5 normal embryos, the wall of the hollow lens vesicle consists of fairly uniform columnar cells (Kaufman 1992). Between E11.5 and E12.0, the cells located at the posterior hemisphere of the vesicle begin to synthesize crystallins and elongate, therefore differentiating into primary lens fibers, which increase progressively in length and make contact with the anterior lens epithelium by E13.0. As a result, the lumen of the lens vesicle is obliterated.

In *R/H* mutants, examination of eye lenses in sagittal and coronal sections at E13.5–17.5 showed that, in contrast to the wild type, contact between the anterior surface of the fiber cell mass and the interior surface of the lens epithelium was not established, leaving behind a portion of unfilled lumen (Fig. 3N–Q). This space has the appearance of a large ''vacuole'' in coronal sections of the eye (eight of eight specimens; see Fig. 3O). In *R/H* mutants affected more severely, abnormal suturing patterns were also observed. Occasionally, a few nuclei were detected in regions of the fiber cell mass that was nuclei-free in wild-type embryos. In addition, the monolayer of lens epithelium was found to be poorly organized (Fig. 3, cf. S with R). Lens defects were minor in *R* embryos of the same ages (only one of three specimens examined exhibited a small lens ''vacuole''). Of the wild-type and *H* embryos examined histologically at E16.5 and E17.5 (five and four specimens, respectively), none exhibited a lens phenotype.

Igf2 is not expressed in the lens (Cuthbertson et al. 1989), whereas *Igf1r* is expressed in several regions of the eye, including the lens (Burren et al. 1996). Thus, the lens abnormalities observed in *R/H* mutants may be the consequence of excessive stimulation of IGF1R by IGF-II, which is known to be present in aqueous and vitreous humor (Arnold et al. 1993; Meyer-Schwickerath et al. 1993).

The lens phenotype of *R/H* embryos is remarkably similar morphologically to that observed in $p57^{KIP2}$ mutants (Zhang et al. 1997). On the other hand, ophthalmologic examinations of BWS and SGBS patients, whenever recorded, did not reveal lens abnormalities (Table 1).

Adrenal abnormalities

Because *Igf2* is expressed in adrenals at a high level (for review, see Mesiano and Jaffe 1997) and adrenocortical cytomegaly and presence of adrenal cysts have been described frequently in BWS (Table 1), we examined the adrenal glands in sagittal sections of E16.5 embryos. Cortical cytomegaly was not observed in any class of mutants, in contrast with $p57^{KIP2}$ null mice (Zhang et al. 1997). Cysts, however, were clearly evident in three of four *R/H* mutants (Fig. 3U). Smaller and fewer cysts were also detected in one of three *R* mutants, but not in wild-type (Fig. 3T) or H embryos (five specimens each). Whereas both cortical and medullary cystic abnormalities were observed in *R/H* mutants, the cysts found in BWS patients are located mostly in the adrenal cortex and can occasionally expand to large size by hemorrhage or accumulation of fluid (see, e.g., McCauley et al. 1991). Therefore, we cannot exclude the possibility that the two sets of observations are unrelated, although such a coincidence appears to be unlikely.

Mutant phenotypes are caused by excess of IGF-II

To examine whether the relative severity of mutant phenotypes (*R/H* > *R* > *H*) could be correlated with corresponding increases in IGF-II, we measured comparatively tissue and serum IGF-II levels by Western analysis (see Materials and Methods). Relative amounts of IGF-II in protein extracts from whole embryos were assayed at E12.5, because a similar analysis (Ludwig et al. 1996) had revealed that in *R* embryos of this age the mutant to wild-type IGF-II ratio was ~2.0, but declined to 1.4 at E13.5. We observed that this ratio was again ~2.0 in E12.5 *R* mutants, and did not differ from that obtained for *H* mutants (Table 5A). In *R/H* mutants, however, the corresponding value was very high (~7.5). Similar assays for serum IGF-II were performed with E14.5 embryos, because this is the earliest age that adequate blood volumes can be collected. In this case, the level of IGF-II was not significantly higher than normal in *H* mutants, but it was increased in the serum of *R* mutants (approximately fourfold the normal amount; Table 5B). Similarly to the tissue extracts, an extremely high level of serum IGF-II was observed in *R/H* mutants (increase >11-fold over normal; Table 5B).

Table 5. *Assay data*

	Normal	*H*	*R*	*R/H*
A. IGF-II in embryonic extracts (E12.5)				
Mutant/wild-type ratio[a]		2.06 ± 0.23	2.11 ± 0.44	7.56 ± 1.76
B. Serum IGF-II (E14.5)				
ng/ml[b]	143 ± 25	163 ± 14	609 ± 75	1672 ± 130
Mutant/wild-type ratio		1.14 ± 0.1	4.25 ± 0.5	11.67 ± 0.9
C. Percent BrdU-positive nuclei[c] (E13.5)				
Kidney	49.8 ± 0.9	47.7 ± 1.1	47.7 ± 1.2	48.6 ± 1.1
Liver	50.9 ± 1.7	58.3 ± 0.6	58.4 ± 1.2	68.4 ± 0.8
Heart	18.6 ± 1.0	24.7 ± 0.8	29.6 ± 1.2	38.1 ± 1.6

[a]Ratios were calculated from normalized arbitrary values (see Materials and Methods).
[b]Averages of four samples per embryo class (ng equivalents of human recombinant IGF-II).
[c]Averages of nine determinations (three embryos per class; three microscopic fields per specimen).

Presently, in the absence of a more detailed developmental analysis of IGF-II levels that would include assays in serum and in individual organs, it is unwarranted to derive conclusions about the particular roles of circulating and locally-produced IGF-II, alone or in combination, in the manifestation of mutant phenotypes. Nevertheless, the relative severity of the *R* and *R/H* phenotypes is strongly correlated overall with a corresponding degree of IGF-II excess. On the other hand, the situation with *H* mutants is less obvious, and a plausible interpretation that their phenotype is relatively mild because there is excess of IGF-II in tissues, but not in serum, is probably simplistic. The observation that serum IGF-II is not elevated in *H* mutants was not totally unexpected, because imprint relaxation of the maternal *Igf2* allele is only partial in liver that secretes this ligand in the circulation (transcriptional output 27% that of the paternal allele; Leighton et al. 1995b). The current lack of information about other mechanistic aspects of IGF-II physiology, however, precludes a straightforward explanation for the interesting observation that the combined actions of the *Igf2r* and *ΔH19* mutations exhibit a remarkable degree of synergism in elevating IGF-II in the serum and tissues of *R/H* embryos.

To examine further whether relative increases of IGF-II in the mutants could be correlated with cellular hyperproliferation, the incorporation of 5′-bromo-2′-deoxyuridine (BrdU) into DNA was assayed in tissue sections of E13.5 embryos (see Materials and Methods). In the kidney, differences in averaged percentages of BrdU-positive nuclei were not detected (Table 5C). This is consistent with the observation that even a day later (E14.5; see allometric analysis above) the average kidney weights were practically identical in all classes of embryos. In the liver, a statistically significant difference in the BrdU score was observed between the wild-type and all of the mutant embryos. There was no difference, however, between *H* and *R* embryos, whereas the value for *R/H* mutants was significantly higher (Table 5C). Finally, proliferation was distinct for each class of embryos in the heart (normal $H < R < R/H$; Table 5C), and the differences between values were statistically significant in all pairwise comparisons.

To support the conclusion that in *R/H* double mutants the biallelic transcription of *Igf2* due to the *ΔH19* mutation aggravates the *R* phenotype, and to demonstrate conclusively that the combined effects of IGF-II overexpression are causally and solely responsible for the *R/H* phenotypic manifestations, we performed genetic experiments by reasoning as follows. In double heterozygotes possessing a maternally inherited *ΔH19* mutation and a paternally inherited *Igf2* mutation (*H/II* double mutants), *Igf2* is expressed only from the intact maternal allele that becomes transcriptionally active by imprint relaxation. Therefore, because the IGF-II dosage is ~1×, there is no manifestation of overgrowth, and these double mutants do not differ phenotypically from wild-type mice (Leighton et al. 1995b). A second consideration was that in *R* mutants maintaining *Igf2* imprinting, the IGF-II transcriptional dosage is also 1× (from the paternal allele), but becomes detrimental because of lack of turnover, as evidenced by the rescue of the *R* mutants in *Igf2* null background (Ludwig et al. 1996). Therefore, if the biallelic *Igf2* expression in *R/H* mutants were reduced to monoallelic, the severity of the *R/H* phenotype should also be reduced to that of the *R* phenotype.

To test this prediction, we generated triple *R/H/II* mutants, in which *Igf2* should be transcribed monoallelically as in *R* mutants, but from the maternal rather than the paternal allele. Thus, we crossed *Igf2r*(+/−)/*ΔH19*(−/−) females with *Igf2(−/−)* males, to derive progeny with two genotypes—*Igf2r*(+/+)/*ΔH19*(*m*−/+)/*Igf2*(+/*p*−), that is, phenotypically normal *H/II* mutants, and *Igf2r*(*m*−/+)/*ΔH19*(*m*−/+)/*Igf2*(+/*p*−) triple mutants. Examination of two litters of embryos at E18.5, a time at which live *R/H* mutants were never recovered, showed that six of nine *R/H/II* triple mutants were alive. Importantly, all nine of these triple mutant embryos lacked typical manifestations of *R/H* mutants. Thus, they had closed eyelids, lacked omphalocele and cleft palate, and their polydactyly (postaxial only), instead of involving at least both forelimbs, was confined to a single forelimb. Moreover, the live triple mutants resembled *R* mutants in terms of average weight (135 ± 6.8% of the weight of normal *H/II* siblings, instead of the characteristic 200% size of *R/H* embryos). Similar to *R* mutants, *R/H/II* animals are apparently unable to survive postnatally (in a litter examined immediately after birth, two dead neonates were recovered and shown by genotyping to be *R/H/II* triple mutants).

Concluding remarks

We have provided strong genetic evidence demonstrating that IGF-II overexpression is causally related to phenotypic manifestations in mouse embryos that bear striking similarities to some features of two human overgrowth disorders, BWS and SGBS. When mouse mutants on the one hand and BWS and SGBS patients on the other are compared, however, conclusions should be drawn with caution, as the genetic lesions are not identical and crucial information pertaining to potentially similar pathogenetic mechanisms is still lacking for both syndromes.

First, it is unknown whether the IGF-II polypeptide is consistently increased in BWS human embryos. To our knowledge, there is only a single measurement of serum IGF-II in a 30-week-old BWS fetus (Lutton et al. 1996) demonstrating a 2.5- to 4-fold increase over the normal concentration range for this particular gestational age (Lassarre et al. 1991; Reece et al. 1994). Postnatally, however, only three of 27 BWS patients examined (0 to 14 years of age) exhibited serum IGF-II levels exceeding significantly normal levels (Schneid et al. 1997). Although it cannot be excluded that the level of IGF-II was abnormally high during gestation, but was somehow downregulated postnatally in the majority of these cases, additional uncertainties exist. For example, reverse transcriptase (RT)–PCR analyses demonstrated imprint relaxation and biallelic IGF-II expression in the tissues of

four young children (three of them with birthweights above the 97th centile), which exhibited somatic overgrowth, but no other diagnostic features of BWS (Morison et al. 1996). The level of IGF-II polypeptide was not measured in this study, but one interpretation of the data is that a presumptive excess of embryonic IGF-II resulting in high birthweight may not be sufficient alone for the complete manifestation of BWS. Nevertheless, considering that BWS is genetically and clinically heterogeneous, but linked to *IGF2*, we think that the remarkable phenotypic simulation caused by IGF-II excess as a consequence of the *R/H* mutations cannot be coincidental, but rather provides evidence supporting an IGF-II involvement in at least some aspects of BWS pathogenesis. Interestingly, other aspects can be attributed to lack of $p57^{KIP2}$ function.

Of the predominant features of BWS, the phenotype of *R/H* mutants can explain somatic overgrowth, including visceromegaly and placentomegaly, and also the occurrence of omphalocele. In regard to this latter feature, the presence of umbilical hernia in $p57^{KIP2}$ mutants indicates that impairment of this function could be a contributing factor to the abdominal wall defects characterizing BWS. Neither the *R/H* nor the $p57^{KIP2}$ mutations, however, can account for the almost invariant manifestation of macroglossia in BWS. It remains to be seen, whether another gene in the 11p15.5 region could be responsible for this manifestation. Alternatively, given the high level of IGF-II expression in the tongue, excess of this factor may be responsible for macroglossia manifested in humans, but not in mice because of dissimilar developmental timing (see Louvi et al. 1997, for a discussion of this topic). Two frequent BWS features, renal dysplasia and adrenal cytomegaly, can be accounted for by lack of $p57^{KIP2}$ alone, as the *R/H* mice do not exhibit these abnormalities. On the other hand, the *R/H*, but not the $p57^{KIP2}$ mutant phenotype can apparently account for cardiac defects and potentially for the occurrence of adrenal cysts in BWS. An interesting, but puzzling observation is that the lens phenotype, which the *R/H* and $p57^{KIP2}$ mutants share, was never described in BWS. Overall, however, when both the overlapping and distinct phenotypic manifestations of the two mutant mouse models are considered altogether, they appear to simulate BWS quite closely. It remains to be seen, however, whether $p57^{KIP2}$ and IGF-II have also a functional relationship in some pathways, beyond the linkage of the corresponding genes in the 11p15.5 region.

In contrast to BWS, the pathogenetic relationship between SGBS patients and *R/H* mutants is tentative and based indirectly on phenotypic similarities, in conjunction with preliminary biochemical evidence suggesting an interaction between IGF-II and human glypican-3 (Pilia et al. 1996). Conclusive evidence, however, is currently lacking, because the biochemical data were not reproduced with the rat GPC3 homolog (OCI-5), for unknown reasons (Song et al. 1997). Nevertheless, in view of the clinical overlap of BWS and SGBS, a tissue-specific increase of IGF-II, when the GPC3-dependent sequestration or down-regulation of this effector is eliminated by mutation of the cognate gene in SGBS, remains an interesting and testable conjecture. At present, this model appears to be consistent with some of the features of the *R/H* mutant phenotype, including somatic overgrowth and organomegaly, heart defects, polydactyly, vertebral anomalies and cleft palate that appear in SGBS with relatively high frequency.

Materials and methods

Mice

The strains of mice used in this study, which carry targeted mutations in the *Igf2r, H19,* and *Igf2* loci, have been described previously (see, respectively, Ludwig et al. 1996; Leighton et al. 1995b; DeChiara et al. 1990). Details of the genetic crosses to generate double and triple mutants are described in the text.

Genotyping

For genotyping, DNA was prepared as described (Hogan et al. 1994) from the yolk sac of E12.5–18.5 embryos or the tail tip of adult mice. The *Igf2r* and *ΔH19* mutations were detected by Southern analysis as described (see, respectively, Ludwig et al. 1996; Leighton et al. 1995b), whereas PCR analysis performed as described (Louvi et al. 1997) was used for detection of the *Igf2* mutation.

Histological and anatomical analyses

For histology, embryos were fixed overnight in Z-fix solution (buffered zinc formalin; Analtech), washed for 24 hr at 4°C in 0.25 M sucrose, 0.2 M glycine, 0.1 M phosphate buffer (pH 7.3), dehydrated, cleared with toluene and embedded in paraffin. Paraffin blocks were sectioned at 5–6 μm and stained with hematoxylin and eosin. Immunohistochemisty was performed using a rat monoclonal antibody against mouse CD31/PECAM-1 (MEC13.3; Pharmingen) and a tyramide amplification kit (Dupont NEN) as recommended by the manufacturers. Slides were counterstained with hematoxylin.

For skeletal analysis essentially as described (Kaufman 1992), fixed embryos were eviscerated, fixed again in 95% ethanol for 1 day, and then stained with 0.015% alcian blue 8GS for 1 day. They were then washed in 95% ethanol for 6 hr and transferred to 2% KOH for 1–2 days before staining with 0.005% alizarin red S overnight. The tissues were cleared with 1% KOH/20% glycerol for several weeks and the skeletons were stored in glycerol.

BrdU labeling of embryos

For labeling of embryonic cells in the S phase with BrdU, pregnant females were injected intraperitoneally with BrdU and 5 fluoro-2′-deoxyuridine (100 μg and 6.7 μg per gram body weight, respectively) at E13.5 and sacrificed 1 hr later. Dissected embryos were fixed, embedded in paraffin and sectioned as described above. Sections were incubated with 0.25% trypsin for 15 min at 37°C, washed with PBS, treated with 4 M HCl for 20 min, washed extensively with PBS, and blocked with 0.5% BSA in PBS. Detection was with a monoclonal anti-BrdU antibody (Sigma) diluted 1:1000 and an alkaline phosphatase-conjugated secondary antibody (Sigma) diluted 1:100. NBT/BCIP reagent (Boehringer) was used for color development and the slides were counterstained with Weigert's hematoxylin. In examined tissues (heart ventricular wall, liver, and kidney), nuclei were

counted in three microscopic fields per section using three embryos of each genotype (total of nine determinations per tissue of each embryo class). Values were expressed as percentages of total nuclei that were BrdU positive. To determine statistically significant differences in pairwise comparisons of these and other data, we used Student's *t*-test ($P < 0.05$).

Measurement of IGF-II levels

Relative amounts of IGF-II in embryonic extracts (E12.5) or serum (E14.5) were determined by Western analysis using a modification of a procedure that we described previously (Ludwig et al. 1996). In these IGF-II assays that are based on electrophoretic analysis, there is no interference by IGF binding proteins. For preparation of protein extracts, whole embryos were homogenized in 1 M acetic acid and the homogenates were incubated on ice for 2 hr, centrifuged, and then neutralized with 5 N NaOH. After protein precipitation with acetone, the pellet was washed with 80% ethanol and resuspended in SDS-PAGE loading buffer. Approximate amounts of total protein in aliquots of these extracts were then determined by preliminary electrophoretic analysis and coomassie blue staining. Samples containing similar amounts of protein were analyzed by SDS-PAGE in parallel with a series of dilutions of human recombinant IGF-II standard (GIBCO), followed by Western analysis as described (Ludwig et al. 1996). To correct for equal loading of protein, membranes were stripped and analyzed by Western blotting using a rabbit polyclonal antibody against HMG-I(Y) (a gift from Dr. D. Thanos, Columbia University). To determine circulating levels of IGF-II, serum samples (5 µl each) were mixed directly with loading buffer before electrophoresis in parallel with dilutions of IGF-II standard. After treatment of membranes with enhanced chemiluminescence (ECL) detection reagents (Amersham) and exposure to X-ray film, signal intensities were measured with a scanning densitometer. In serum, three species of IGF-II (7, 10, and 12 kD) were identified, whereas only two of them (7 and 10 kD) were detected in extracts. Controls verified the authenticity of these molecular forms, as they were absent from serum and extracts of *Igf2* null embryos. For each sample, the sum of densitometric values of IGF-II species was considered as the total amount of IGF-II. Serum IGF-II values were expressed as nanogram equivalents of recombinant human IGF-II per milliliter on the basis of the standard curve. For extracts, arbitrary IGF-II values were first normalized to the HMG-I(Y) standard and then mutant/wild-type ratios were calculated for littermates. A final average ratio was derived from the data from three litters of embryos (one embryo of each genotype per litter).

Growth analysis

For staging of embryos, we considered the noon of the day of vaginal plug appearance as E0.5. For developmental analysis of growth, embryos and their placentas were dissected and fixed in Z-fix. For measurements of organ weights, individual organs were dissected from fixed embryos and stored in fixative. Specimens were patted dry with absorbent paper prior to weight determination with a microbalance.

Regression analyses (plots of weight versus age) by application of a Gompertz equation (see Laird et al. 1965) were performed by a curve-fitting computer program (SigmaPlot) using for each class of embryos average weights at each time point. In the Gompertz function $W = A \exp[-b \exp(-kt)]$, W and A are the weight at time t and the asymptotic weight, respectively, while b and k are constants. This mathematical treatment takes into consideration that the specific rate $(1/W) \times (dW/dt)$ of the exponential embryonic growth is not constant, but declines exponentially (Laird et al. 1965).

To determine the allometric relationship between organ weights (OW) and embryonic body weights (BW) measured at different developmental ages, we used regression analyses of log–log plots according to the allometric equation $\log(OW) = \log a + b \log(BW)$, where b is the slope of the regression line relating OW and BW and a is the *y*-axis intercept (see, e.g., Shea et al. 1987). The results of regressions were compared between embryo classes by analysis of covariance as described (Mellits 1968), to assess differences in slope and/or position of regression lines ($P < 0.05$). For a particular organ, simple extension of the regression line of the wild-type control by the corresponding line of a mutant indicated a common trajectory of relative growth, whereas significant statistical differences in slope or position of lines were interpreted as reflecting deviations from normal allometry (for further details, see text).

Acknowledgments

We thank Joe Terwilliger for help with the statistical analyses of allometry; Sanjay Shirke and Richard Lang for advice on lens histopathology; Dimitris Thanos for reagents; and Ed Laufer for discussions. This work was supported by National Institutes of Health grants HD34526 and MH50733 (Project 2) to A.E.

The publication costs of this article were defrayed in part by payment of page charges. This article must therefore be hereby marked ''advertisement'' in accordance with 18 USC section 1734 solely to indicate this fact.

References

Achiron, R., D. Soriano, S. Lipitz, S. Mashiach, B. Goldman, and D.S. Seidman. 1995. Fetal midgut herniation into the umbilical cord: Improved definition of ventral abdominal anomaly with the use of transvaginal sonography. *Ultrasound Obstet. Gynecol.* **6:** 256–260.

Amann, G. and F.S. Sherman. 1992. Myocardial dysgenesis with persistent sinusoids in a neonate with Noonan's phenotype. *Pediatr. Path.* **12:** 83–92.

Arnold, D.R., P. Moshayedi, T.J. Schoen, E. Jones, G.J. Chader, and R.J. Waldbillig. 1993. Distribution of IGF-I and -II, IGF binding proteins (IGFBPs) and IGFBP mRNA in ocular fluids and tissues: Potential sites of synthesis of IGFBPs in aqueous and vitreous. *Exp. Eye Res.* **56:** 555–565.

Barlow, D.P., R. Stöger, B.G. Hermann, K. Saito, and N. Schweifer. 1991. The mouse insulin-like growth factor type-2 receptor is imprinted and closely linked to the *Tme* locus. *Nature* **349:** 84–87.

Bartolomei, M.S., S. Zemel, and S.M. Tilghman. 1991. Parental imprinting of the mouse *H19* gene. *Nature* **351:** 153–155.

Bartolomei, M.S., A.L. Webber, M.E. Brunkow, and S.M. Tilghman. 1993. Epigenetic mechanisms underlying the imprinting of the mouse *H19* gene. *Genes & Dev.* **7:** 1663–1673.

Beckwith, J.B. 1969. Macroglossia, omphalocele, adrenal cytomegaly, gigantism, and hyperplastic visceromegaly. *Birth Defects* **V(2):** 188–196.

Beechey, C.V., S.T. Ball, K.M.S. Townsend, and J. Jones. 1997. The mouse chromosome 7 distal imprinting domain maps to G-bands F4/F5. *Mamm. Genome* **8:** 236–240.

Behmel, A., E. Plöchl, and W. Rosenkranz. 1984. A new X-linked dysplasia gigantism syndrome: Identical with the Simpson dysplasia syndrome? *Hum. Genet.* **67:** 409–413.

———. 1988. A new X-linked dysplasia gigantism syndrome: Follow up in the first family and report of a second Austrian family. *Am. J. Med. Genet.* **30:** 275–285.

Brown, K.W., A. Gardner, J.C. Williams, M.G. Mott, A.McDermott, and N.J. Maitland. 1991. Paternal origin of 11p15 duplications in the Beckwith-Wiedemann syndrome. A new case and review of the literature. *Cancer Genet. Cytogenet.* **58:** 66–70.

Brutsaert, D.L. and L.J. Andries. 1992. The endocardial endothelium. *Am. J. Physiol.* **263:** H985–H1002.

Burren, C.P., J.L. Berka, S.R. Edmondson, G.A. Werther, and J.A. Batch. 1996. Localization of mRNAs for insulin-like growth factor-I (IGF-I), IGF-I receptor, and IGF binding proteins in rat eye. *Invest. Ophthalmol. Vis. Sci.* **37:** 1459–1468.

Chen, E., J.P. Johnson, V.A. Cox, and M. Golabi. 1993. Simpson-Golabi-Behmel syndrome: Congenital diaphragmatic hernia and radiologic findings in two patients and follow-up of a previously reported case. *Am. J. Med. Genet.* **46:** 574–578.

Chen, J.M. 1952. Studies on the morphogenesis of the mouse sternum. I. Normal embryonic development. *J. Anat.* **86:** 373–389.

Cohn, M.J. and C. Tickle. 1996. Limbs: A model for pattern formation within the vertebrate body plan. *Trends Genet.* **12:** 253–257.

Cuthbertson, R.A., F. Beck, P.V. Senior, J. Haralambidis, J.D. Penschow, and J.D. Coghlan. 1989. Insulin-like growth factor II may play a local role in the regulation of ocular size. *Development* **107:** 123–130.

DeChiara, T.M., A. Efstratiadis, and E.J. Robertson. 1990. A growth-deficiency phenotype in heterozygous mice carrying an insulin-like growth factor II gene disrupted by targeting. *Nature* **345:** 78–80.

DeChiara, T.M., E.J. Robertson, and A. Efstratiadis. 1991. Parental imprinting of the mouse insulin-like growth factor II gene. *Cell* **64:** 849–859.

Dollé, P., A. Dierich, M. LeMeur, T. Schimmang, B. Schuhbauer, P. Chambon, and D. Duboule. 1993. Disruption of the Hoxd-13 gene induces localized heterochrony leading to mice with neotenic limbs. *Cell* **75:** 431–441.

Duhamel, B. 1963. Embryology of exomphalos and allied malformations. *Arc. Dis. Childh.* **38:** 142–147.

Elliot, M. and E.R. Maher. 1994. Beckwith-Wiedemann syndrome. *J. Med. Genet.* **31:** 560–564.

Elliot, M., R. Bayly, T. Cole, I.K. Temple, and E.R. Maher. 1994. Clinical features and natural history of Beckwith-Wiedemann syndrome: Presentation of 74 new cases. *Clin. Genet.* **46:** 168–174.

Engström, W., S. Lindham, and P. Schofield. 1988. Beckwith-Wiedemann syndrome. *Eur. J. Pediatr.* **147:** 450–457.

Ferguson, M.W.J. 1988. Palate development. *Development* (Suppl.) **103:** 41–60.

Ferguson, M.W.J., P.M. Sharpe, B.L. Thomas, and F. Beck. 1992. Differential expression of insulin-like growth factors I and II (IGF I and II), mRNA, peptide and binding protein 1 during mouse palate development: Comparison with TGFβ peptide distribution. *J. Anat.* **181:** 219–238.

Filipi, G. and V.A. McKusick. 1970. The Beckwith-Wiedemann syndrome (the exomphalos-macroglossia-gigantism syndrome). Report of two cases and review of the literature. *Medicine* **40:** 279–298.

Garganta, C.L. and J.N. Bodurtha. 1992. Report of another family with Simpson-Golabi-Behmel syndrome and a review of the literature. *Am. J. Med. Genet.* **44:** 129–135.

Giannoukakis, N., C. Deal, J. Paquette, C.G. Goodyer, and C. Polychronakos. 1993. Parental genomic imprinting of the human *IGF2* gene. *Nature Genet.* **4:** 98–101.

Golabi, M. and L. Rosen. 1984. A new X-linked mental retardation-overgrowth syndrome. *Am. J. Med. Genet.* **17:** 345–358.

Greenwood, R.D., A. Sommer, A. Rosenthal, J. Craenen, and A.S. Nadas. 1977. Cardiovascular abnormalities in the Beckwith-Wiedemann syndrome. *Am. J. Dis. Child.* **131:** 293–294.

Gurrieri, F., M. Cappa, and G. Neri. 1992. Further delineation of the Simpson-Golabi-Behmel (SGB) syndrome. *Am. J. Med. Genet.* **44:** 136–137.

Harris, M.J. and M.J. McLeod. 1982. Eyelid growth and fusion in fetal mice. *Anat. Embryol.* **164:** 207–220.

Hatada, I., H. Ohashi, Y. Fukushima, Y. Kaneko, M. Inoue, Y. Komoto, A. Okada, S. Ohishi, A. Nabetani, H. Morisaki, M. Nakayama, N. Niikawa, and T. Mukai. 1996. An imprinted gene $p57^{KIP2}$ is mutated in Beckwith-Wiedemann syndrome. *Nature Genet.* **14:** 171–173.

Henry, I., C. Bonaïti-Pellié, V. Chehensse, C. Beldjord, C. Schwartz, G. Utermann, and C. Junien. 1991. Uniparental paternal disomy in a genetic cancer-predisposing syndrome. *Nature* **351:** 665–667.

Hogan, B., R. Beddington, F. Costantini, and E. Lacy. 1994. *Manipulating the mouse embryo: A laboratory manual.* Cold Spring Harbor Laboratory Press, Cold Spring Harbor, NY.

Hughes-Benzie, R.M., A.G.W. Hunter, J.E. Allanson, and A.E. Mackenzie. 1992a. Simpson-Golabi-Behmel syndrome associated with renal dysplasia and embryonal tumor: Localization of the gene to Xqcen-q21. *Am. J. Med. Genet.* **43:** 428–435.

Hughes-Benzie, R., J. Allanson, A. Hunter, and T. Cole. 1992b. The importance of differentiating Simpson-Golabi-Behmel and Beckwith-Wiedemann syndromes. *J. Med. Genet.* **29:** 928.

Hughes-Benzie, R.M., J.L. Tolmie, M. McNay, and A. Patrick. 1994. Simpson-Golabi-Behmel syndrome: Disproportionate fetal overgrowth and elevated maternal serum alpha-fetoprotein. *Prenatal Diag.* **14:** 313–318.

Hughes-Benzie, R.M., G. Pilia, J.Y. Xuan, A.G.W. Hunter, E. Chen, M. Golabi, J.A. Hurst, J. Kobori, K. Marymee, R.A. Pagon, H.H. Punnett, S. Schelley, J.L. Tolmie, M.M. Wohlferd, T. Grossman, D. Schlessinger, and A.E. MacKenzie. 1996. Simpson-Golabi-Behmel syndrome: Genotype/phenotype analysis of 18 affected males from 7 unrelated families. *Am. J. Med. Genet.* **66:** 227–234.

Icardo, J.M. and F.J. Manasek. 1992. Cardiogenesis: Development mechanisms and embryology. In *The heart and cardiovascular system* (ed. H.A. Fozzard et al.), Vol. II, pp. 1563–1586. Raven Press, New York, NY.

Irving, I.M. 1967. Exomphalos with macroglossia: A study of eleven cases. *J. Pediatr. Surg.* **2:** 499–507.

Journel, H., J. Lucas, C. Allaire, F. Le Mée, G. Defawe, M. Lecornu, H. Jouan, M. Roussey, and B. Le Marec. 1985. Trisomy 11p15 and Beckwith-Wiedemann syndrome. *Ann. Genet.* **28:** 97–101.

Kaufman, M.H. 1992. *The atlas of mouse development.* Academic Press, San Diego, CA.

König, R., S. Fuchs, C. Kern, and U. Langenbeck. 1991. Simpson-Golabi-Behmel syndrome with severe cardiac arrhythmias. *Am. J. Med. Genet.* **38:** 244–247.

Kosseff, A., J. Herrmann, E.F. Gilbert, C. Viseskul, M. Lubinsky, and J.M. Opitz. 1976. Studies of malformation syndromes in man XXIX: The Wiedemann-Beckwith syndrome. Clinical, genetic and pathogenetic studies of 12 cases. *Eur. J. Pediatr.* **123:** 139–166.

Koufos, A., P. Grundy, K. Morgan, K.A. Aleck, T. Hadro, B.C. Lampkin, A. Kalbakji, and W.K. Cavenee. 1989. Familial Beckwith-Wiedemann syndrome and a second Wilms tumor locus both map to 11p15.5. *Am. J. Hum. Genet.* **44:** 711–719.

Kubota, T., S. Saitoh, T. Matsumoto, K. Narahara, Y. Fukushima, Y. Jinno, and N. Niikawa. 1994. Excess functional

copy of allele at chromosomal region 11p15 may cause Wiedemann-Beckwith (EMG) syndrome. *Am. J. Med. Genet.* **49:** 378–383.

Laird, A.K., S.A. Tyler, and A.D. Barton. 1965. Dynamics of growth. *Growth* **29:** 233–248.

Lassarre, C., S. Hardouin, F. Daffos, F. Forestier, F. Frankenne, and M. Binoux. 1991. Serum insulin-like growth factors and insulin-like growth factor binding proteins in the human fetus. Relationships with growth in normal subjects and in subjects with intrauterine growth retardation. *Pediatr. Res.* **29:** 219–225.

Lau, M.M.H., C.E.H. Stewart, Z. Liu, H. Bhatt, P. Rotwein, and C.L. Stewart. 1994. Loss of the imprinted IGF2/cation-independent mannose 6-phosphate receptor results in fetal overgrowth and perinatal lethality. *Genes & Dev.* **8:** 2953–2963.

Laufer, E. 1993. Factoring in the limb. *Curr. Biol.* **3:** 306–308.

Lee, F.A. 1972. Radiology of the Beckwith-Wiedemann syndrome. *Radiol. Clin. North Am.* **10:** 261–276.

Lee, M.P., M. DeBaun, G. Randhawa, B.A. Reichard, S.J. Elledge, and A.P. Feinberg. 1997. Low frequency of $p57^{KIP2}$ mutation in Beckwith-Wiedemann syndrome. *Am. J. Hum. Genet.* **61:** 304–309.

Leighton, P.A., J.R. Saam, R.S. Ingram, C.L. Stewart, and S.M. Tilghman. 1995a. An enhancer deletion affects both *H19* and *Igf2* expression. *Genes & Dev.* **9:** 2079–2089.

Leighton, P.A., R.S. Ingram, J. Eggenschwiler, A. Efstratiadis, and S.M. Tilghman. 1995b. Disruption of imprinting caused by deletion of the *H19* gene region in mice. *Nature* **375:** 34–39.

LeRoith, D., H. Werner, D. Beitner-Johnson, and C.T. Roberts. 1995. Molecular and cellular aspects of the insulin-like growth factor I receptor. *Endocr. Rev.* **16:** 143–163.

Louvi, A., D. Accili, and A. Efstratiadis. 1997. Growth-promoting interaction of IGF-II with the insulin receptor during mouse embryonic development. *Dev. Biol.* **189:** 33–48.

Ludwig, T., R. Le Borgne, and B. Hoflack. 1995. Roles of mannose-6-phosphate receptors in lysosomal enzyme sorting, IGF-II binding and clathrin-coat assembly. *Trends Cell Biol.* **5:** 202–206.

Ludwig, T., J. Eggenschwiler, P. Fisher, A. J. D'Ercole, M. L. Davenport, and A. Efstratiadis. 1996. Mouse mutants lacking the type 2 IGF receptor (IGF2R) are rescued from perinatal lethality in *Igf2* and *Igf1r* null backgrounds. *Dev. Biol.* **177:** 517–535.

Lutton, D., J. Lepercq, O. Sibony, P. Barbet, Y. Le Bouc, J. Chavinié, and F. Lewin. 1996. Acromegalic pregnancy associated with a Beckwith-Wiedemann fetus. *Fetal Diagn. Ther.* **11:** 154–158.

Martínez y Martínez, R. 1996. Clinical features in the Wiedemann-Beckwith syndrome. *Clin. Genet.* **50:** 272–274.

McCauley, R.G.K., J.B. Beckwith, E.R. Elias, E.N. Faerber, L.H. Prewitt, and W.E. Berdon. 1991. Benign henorrhagic adrenocortical macrocysts in Beckwith-Wiedemann syndrome. *Am. J. Roentgenol.* **157:** 549–552.

McLaren, A. 1965. Genetic and environmental effects on foetal and placental growth in mice. *J. Reprod. Fert.* **9:** 79–98.

McManamny, D.S. and J.S.Barnett. 1985. Macroglossia as a presentation of the Beckwith-Wiedemann syndrome. *Plast. Reconstr. Surg.* **75:** 170–176.

Mellits, D.E. 1968. Statistical methods. In *Human growth: Body composition, cell growth, energy and intelligence* (ed. D.B. Cheek), pp. 19–38. Lea and Febiger, Philadelphia, PA.

Mesiano, S. and R.B. Jaffe. 1997. Role of growth factors in the developmental regulation of the human fetal adrenal cortex. *Steroids* **62:** 62–72.

Meyer-Schwickerath, R., A. Pfeiffer, A. Blum, H. Freyberger, M. Klein, C. Lösche, R. Röllmann, and H. Schatz. 1993. Vitreous levels of the insulin-like growth factors I and II, and the insulin-like growth factor binding proteins 2 and 3, increase in neovascular eye disease. *J. Clin. Invest.* **92:** 2620–2625.

Morison, I.M., D.M. Becroft, T. Taniguchi, C.G. Woods, and C.G. Reeve. 1996. Somatic overgrowth associated with overexpression of insulin-like growth factor II. *Nature Med.* **2:** 311–316.

Neri, G., R. Marini, M. Cappa, P. Borrelli, and J.M. Opitz. 1988. Simpson-Golabi-Behmel syndrome: An X-linked encephalotrophoschisis syndrome. *Am. J. Med. Genet.* **30:** 287–299.

Niikawa, N., S. Ishikiriyama, S. Takahashi, A. Inagawa, H. Tonoki, Y. Ohta, N. Hase, T. Kamei, and T. Kajii. 1986. The Wiedemann-Beckwith syndrome: Pedigree studies on five families with evidence for autosomal dominant inheritance with variable expressivity. *Am. J. Med. Genet.* **24:** 41–55.

Nyström, A., J.E. Cheetham, W. Engström, and P.N. Schofield. 1992. Molecular analysis of patients with Wiedemann-Beckwith syndrome. II. Paternally derived disomies of chromosome 11. *Eur. J. Pediatr.* **151:** 511–514.

Ohlsson, R., A. Nyström, S. Pfeifer-Ohlsson, V. Töhönen, F.Hedborg, P. Schofield, F. Flam, and T.J. Ekström. 1993. *IGF2* is parentally imprinted during human embryogenesis and in the Beckwith-Wiedemann syndrome. *Nature Genet.* **4:** 94–97.

O'Keefe, D., D. Dao, L. Zhao, R. Sanderson, D. Warburton, L. Weiss, K. Anyane-Yeboa, and B. Tycko. 1997. Coding mutations in $p57^{KIP2}$ are present in some cases of Beckwith-Wiedemann syndrome but are rare or absent in Wilms tumors. *Am. J. Hum. Genet.* **61:** 295–303.

Opitz, J.M. 1984. The Golabi-Rosen syndrome—report of a second family. *Am. J. Med. Genet.* **17:** 359–366.

Opitz, J.M., J. Herrmann, E.F. Gilbert, and R. Matalon. 1988. Simpson-Golabi-Behmel syndrome: Follow up of the Michigan family. *Am. J. Med. Genet.* **30:** 301–308.

Pettenati, M.J., J.L. Haines, R.R. Higgins, R.S. Wappner, C.G. Palmer, and D.D. Weaver. 1986. Wiedemann-Beckwith syndrome: presentation of clinical and cytogenetic data on 22 new cases and review of the literature. *Hum. Genet.* **74:** 143–154.

Pilia, G., R.M. Hughes-Benzie, A. MacKenzie, P. Baybayan, E.Y. Chen, R. Huber, G. Neri, A. Cao, A. Farabosco, and D. Schlessinger. 1996. Mutations in *GPC3,* a glypican gene, cause the Simpson-Golabi-Behmel overgrowth syndrome. *Nature Genet.* **12:** 241–247.

Ping, A.J., A.E. Reeve, D.J. Law, M.R. Young, M. Boehnke, and A.P. Feinberg. 1989. Genetic linkage of Beckwith–Wiedemann syndrome to 11p15. *Am. J. Hum. Genet.* **44:** 720–723.

Pleeging, J.H. 1977. Die Entwicklung des Darmes bei der Maus. *Acta Morphol. Neerl. Scand.* **15:** 143–158.

Ramesar, R., M. Babaya, and D. Viljoen. 1993. Molecular investigation of familial Beckwith-Wiedemann syndrome: A model for paternal imprinting. *Eur. J. Hum. Genet.* **1:** 109–113.

Ranzini, A.C., D. Day-Salvatore, T. Turner, J.C. Smulian, and A.M. Vintzileos. 1997. Intrauterine growth and ultrasound findings in fetuses with Beckwith-Wiedemann syndrome. *Obstet. Gynecol.* **89:** 538–542.

Reece, E.A., A. Wiznitzer, E. Le, C.J. Homko, H. Behrman, and E.M. Spencer. 1994. The relation between human fetal growth and fetal blood levels of insulin-like growth factors I and II, their binding proteins, and receptors. *Obstet. Gynecol.* **84:** 88–95.

Reik, W. and E.R. Maher. 1997. Imprinting in clusters: Lessons from Beckwith-Wiedemann syndrome. *Trends Genet.* **13:** 330–334.

Rubin, R. and R. Baserga. 1995. Insulin-like growth factor-I receptor: Its role in cell proliferation, apoptosis and tumorigenicity. *Lab. Invest.* **73:** 311–331.

Schneid, H., M.P. Vazquez, M.P. Vacher, M. Gourmelen, S. Cabrol, and S. Le Bouc. 1997. The Beckwith-Wiedemann syndrome phenotype and the risk of cancer. *Med. Pediatr. Oncol.* **28:** 411–415.

Shapiro, L.R., P.A. Duncan, M.M. Davidian, and N. Singer. 1982. The placenta in familial Beckwith-Wiedemann syndrome. *Birth Defects* **18:** 203–206.

Shea, B.T., R.E. Hammer, and R.L. Brinster. 1987. Growth allometry of the organs in giant transgenic mice. *Endocrinology* **121:** 1924–1930.

Simpson, J.L., S. Landey, M. New, and J. German. 1975. A previously unrecognized X-linked syndrome of dysmorphia. *Birth Defects* **11:** 18–24.

Simpson, E.M., C.C. Linder, E.E. Sargent, M.T. Davisson, L.E. Mobraaten, and J.J. Sharp. 1997. Genetic variation among 129 substrains and its importance for targeted mutagenesis in mice. *Nature Genet.* **16:** 19–27.

Song, H.H., W. Shi, and J. Filmus. 1997. OCI-5/rat glypican-3 binds to fibroblast growth factor-2 but not to insulin-like growth factor-2. *J. Biol. Chem.* **272:** 7574–7577.

Sotelo-Avila, C. and D.B. Singer. 1970. Syndrome of hyperplastic fetal visceromegaly and neonatal hypoglycemia (Beckwith's syndrome). *Pediatrics* **46:** 240–251.

Sotelo-Avila, C., F. Gonzalez-Crussi, and J.W. Fowler. 1980. Complete and incomplete forms of Beckwith-Wiedemann syndrome. Their oncogenic potential. *J. Pediatr.* **96:** 47–50.

Streck, R.D., T.L. Wood, M.-S. Hsu, and J.E. Pintar. 1992. Insulin-like growth factor I and II and insulin-like growth factor binding protein-2 are expressed in adjacent tissues within rat embryonic and fetal limbs. *Dev. Biol.* **151:** 586–596.

Takato, T., M. Kamei, K. Kato, and I. Kitano. 1989. Cleft palate in the Beckwith-Wiedemann syndrome. *Ann. Plast. Surg.* **22:** 347–349.

Takayama, M., H. Soma, S. Yaguchi, H. Funayama, K. Fujiwara, H. Irie, and S. Yamabe. 1986. Abnormally large placenta associated with Beckwith-Wiedemann syndrome. *Gynecol. Obstet. Invest.* **22:** 165–168.

Temtamy, S.A. and V.A. McKusick. 1978. The genetics of hand malformations. *Birth Defects* **14:** 364–392.

Thorburn, M.J., E.S. Wright, C.G. Miller, and E.H. McNeil Smith-Read. 1970. Exomphalos-macroglossia-gigantism syndrome in Jamaican infants. *Am. J. Dis. Child.* **119:** 316–321.

Tsukahara, M., S. Tanaka, and T. Kajii. 1984. A Weaver-like syndrome in a Japanese boy. *Clin. Genet.* **25:** 73–78.

Turleau, C., and J. de Grouchy. 1985. Beckwith-Wiedemann syndrome. Clinical comparison between patients with and without 11p15 trisomy. *Ann. Genet.* **28:** 93–96.

Verloes, A., B. Massart, I. Dehalleux, J.-P. Langhendries, and L. Koulischer. 1995. Clinical overlap of Beckwith-Wiedemann, Perlman and Simpson-Golabi-Behmel syndromes: A diagnostic pitfall. *Clin. Genet.* **47:** 257–262.

Vermeij-Keers , C., N.G. Hartwig, and J.F.A. van der Wefrr. 1996. Embryonic development of the ventral body wall and its congenital malformations. *Sem. Pediatr. Surg.* **5:** 82–89.

Wang, Z.-Q., M.R. Fung, D.P. Barlow, and E.F. Wagner. 1994. Regulation of embryonic growth and lysosomal targeting by the imprinted *Igf2/Mpr* gene. *Nature* **372:** 464–467.

Waziri, M., S.R. Patil, J.W. Hanson, and J.A. Bartley. 1983. Abnormality of chromosome 11 in patients of Beckwith-Wiedemann syndrome. *J. Pediatr.* **102:** 873–876.

Weksberg, R. and J.A. Squire. 1996. Molecular biology of Beckwith-Wiedemann syndrome. *Med. Pediatr. Oncol.* **27:** 462–469.

Weksberg, R., J.A. Squire, and D.M. Templeton. 1996. Glypicans: A growing trend. *Nature Genet.* **12:** 225–227.

Weng, E.Y., G.R. Mortier, and J.M. Graham. 1995a. Beckwith-Wiedemann syndrome. An update and review for the primary pediatrician. *Clin. Pediatr.* **34:** 317–326.

Weng, E.Y., J.B. Moeschler, and J.M. Graham. 1995b. Longitudinal observations on 15 children with Wiedemann-Beckwith syndrome. *Am. J.. Med. Genet.* **56:** 366–373.

Wise, T.L. and D.D. Pravtcheva. 1997. Perinatal lethality in *H19* enhancers-*Igf2* transgenic mice. *Mol. Reprod. Dev.* **48:** 194–207.

Witte, D.P. and K.E. Bove. 1994. Beckwith-Wiedemann syndrome and the insulin-like growth factor-II gene. Does the genotype explain the phenotype? *Am. J. Pathol.* **145:** 762–765.

Yamashita, H., I. Yasuhi, T. Ishimaru, T. Matsumoto, and T. Yamabe. 1995. A case of nondiabetic macrosomia with Simpson-Golabi-Behmel syndrome: Antenatal sonographic findings. *Fetal Diagn. Ther.* **10:** 134–138.

Yan, Y., J. Frisén, M.-H. Lee, J. Massagué, and M. Barbacid. 1997. Ablation of the CDK inhibitor $p57^{Kip2}$ results in increased apoptosis and delayed differentiation during mouse development. *Genes & Dev.* **11:** 973–983.

Zemel, S., M.S. Bartolomei, and S.M. Tilghman. 1992. Physical linkage of two mammalian imprinted genes, *H19* and insulin-like growth factor 2. *Nature Genet.* **2:** 61–65.

Zhang, Y. and B. Tycko. 1992. Monoallelic expression of the human H19 gene. *Nature Genet.* **1:** 40–44.

Zhang, P, N.J. Liégeois, C. Wong, M. Finegold, H. Hou, J.C. Thompson, A. Silverman, J.W. Harper, R.A. DePinho, and S.J. Elledge. 1997. Altered cell differentiation and proliferation in mice lacking $p57^{KIP2}$ indicates a role in Beckwith-Wiedemann syndrome. *Nature* **387:** 151–158.